New Journal of Physics
The open access journal at the forefront of physics

Deutsche Physikalische Gesellschaft DPG
IOP Institute of Physics

Published in partnership with: Deutsche Physikalische Gesellschaft and the Institute of Physics

OPEN ACCESS

RECEIVED
16 May 2021

REVISED
25 September 2021

ACCEPTED FOR PUBLICATION
5 October 2021

PUBLISHED
29 October 2021

PAPER

Competing phases and critical behaviour in three coupled spinless Luttinger liquids

S Kundu[1,2,3,*] and V Tripathi[1]

[1] Department of Theoretical Physics, Tata Institute of Fundamental Research, Homi Bhabha Road, Colaba, Mumbai 400005, India
[2] Département de physique and Institut quantique, Université de Sherbrooke, Sherbrooke, Québec, J1K 2R1, Canada
[3] Department of Physics, University of Florida, Gainesville, FL 32611, United States of America
[*] Author to whom any correspondence should be addressed.

E-mail: sarbajay.kundu@ufl.edu

Keywords: Luttinger liquids, bosonization, renormalization group, phase diagram

Abstract

We study electronic phase competition in a strongly correlated system of three coupled spinless Luttinger liquids—one of the simplest models where topologically nontrivial chiral orders may be realized. We study the problem as a coupled sine-Gordon model, using a perturbative renormalization group (RG) approach. In contrast with counterparts with fewer fermionic species, here the scaling procedure generates off-diagonal contributions to the phase stiffness matrix, which require both rescaling as well as large rotations of the bosonic fields. These rotations, generally non-abelian in nature, introduce a coupling between different interaction channels even at the tree-level order in the coupling constant scaling equations. We study competing phases in this system, taking into account the aforementioned rotations, and determine its critical behaviour in a variety of interaction parameter regimes where perturbative RG is possible. The phase boundaries are found to be of the Berezinskii–Kosterlitz–Thouless type, and we specify the parameter regimes where symmetry breaking between the three flavours of bosonic fields, orders involving different flavours, and chiral orders may be observed. Our approach and findings may be relevant for understanding phases and transitions at high magnetic fields in semimetals such as bismuth featuring three Fermi pockets.

1. Introduction

Coupled one-dimensional systems of interacting fermions appear in diverse contexts. They have been used as building blocks for studying higher-dimensional systems, such as cuprate high-temperature superconductors [1–10], due to the availability of controlled nonperturbative methods and numerical techniques for analyzing them. They have also appeared in studies of low-dimensional organic conductors [11], spin ladders [12–19], Mott insulating magnets [20], as well as artificial structures (such as self-assembled transition metal nanowires [21]). Systems of three coupled Luttinger liquids have been studied in the context of carbon nanotube systems [22, 23], three-leg spin-tube models [24–29], coupled fermionic chains appearing in spin-ladder materials [18, 30–33] and quasi-1D superconductors such as $K_2Cr_3As_3$ [34]. The case of three spinless Luttinger liquids is especially interesting since this is the simplest instance where orders such as chiral superconductivity [35] and chiral density wave can be realized, which are not possible for Luttinger liquid systems with fewer fermionic species. Experimentally, understanding the physics of three coupled spinless Luttinger liquids could be useful in the context of multipocket systems such as bismuth [36–47] and graphite intercalates [48, 49] in a strong magnetic field. In the quantum limit, these would behave effectively as spinless one-dimensional systems.

Bosonization [50, 51], together with a scaling treatment, has been a favoured method for studying the low-energy properties of such systems [2, 5–9, 11, 22, 52–57]. For coupled Luttinger liquid systems with three or more fermionic species, the scaling procedure generically introduces off-diagonal corrections to the stiffness matrix $\widehat{K}$ in the quadratic part of the bosonized Hamiltonian (a sine-Gordon model): these

contributions have largely been neglected in the existing analyses [9, 22, 34], and need to be taken into account. They carry information about the competition between different interaction channels, which in turn governs the electronic phase competition and critical behaviour in these systems. Although these corrections have been introduced in a study involving two spinful coupled Luttinger liquids [5], in the context of competing orders in cuprates, the specific nature of the interactions considered there precluded the existence of chiral orders. On the other hand, the simplest situation where such nontrivial corrections arise, is the case of three coupled spinless Luttinger liquids.

In this paper, we study the electronic phases and critical behaviour in strongly correlated systems with effectively three one-dimensional spinless Fermi pockets. The strongly correlated pockets are characterized by the Luttinger $\widehat{K}$-parameters significantly differing from unity. Instabilities of the Luttinger liquid phase are brought about through the introduction of small sine-Gordon couplings. We perform a perturbative renormalization group (RG) analysis for such a system that takes into account the effects of the off-diagonal corrections by introducing large rotations of the $\widehat{K}$-matrix, and small renormalizations of the eigenvalues of $\widehat{K}$. Of these two, the latter affects the scaling dimensions of the interactions, while the former effectively rotates the bosonic fields, which affects the subsequent stages of the scaling. From the solutions of the scaling equations, we identify the most singular susceptibilities, corresponding to different order parameters, which in turn determines the phase diagram. Also, from a numerical scaling analysis of the RG equations, we obtain the critical behaviour near the phase transition points.

Our main findings are as follows. We find that the fixed point behaviour is dependent both on the relative initial values of the sine-Gordon couplings, as well as the Luttinger liquid parameters, and in particular, the scaling behaviour of each coupling is affected by the initial conditions chosen for the other couplings, even at the tree level. This is a situation qualitatively different from that of systems with two or fewer fermionic species, where such an interplay between different interaction channels does not appear at the tree-level order, and is a direct consequence of the rotations of the stiffness matrices introduced in our approach. Depending upon the relative initial values of the couplings and the Luttinger parameters, we identify the different instabilities in the particle–particle (p–p) and particle–hole (p–h) channels, and obtain the conditions under which symmetry breaking between the bosonic flavours and orders involving different flavours may appear in both these channels. The possibility of chiral orders is also discussed in this context. The phase boundaries in the parameter regimes where we performed our analysis were found to be of the Berezinskii–Kosterlitz–Thouless (BKT) type.

The rest of the paper is organized as follows. Section 2 introduces the bosonic Hamiltonian used in our analysis, arising from generic density–density interactions for three spinless fermionic species. Section 3 describes the RG procedure used in our analysis. In section 4, we introduce test vertices corresponding to different order parameter fields and study their evolution under the RG, to determine the possible instabilities in different channels. Finally, section 5 presents a discussion of our results, conclusions and future directions.

2. Bosonic model

We begin with a bosonized Luttinger liquid Hamiltonian with three flavours of Bose fields corresponding to indices $\mu = 0, 1, -1$, consisting of the usual quadratic terms (arising from fermionic interactions of the form $\rho_R\rho_R$, $\rho_L\rho_L$ and $\rho_R\rho_L$, L and R denoting left- and right-moving fermions, respectively), as well as sine-Gordon terms. The latter are responsible for instabilities that may arise in the gapless Luttinger liquid phase, and so we refer to these as 'interactions' in the bosonic picture. The quadratic or 'noninteracting' part has the general form

$$H_0^B = \frac{1}{2}\int dx \sum_{\mu,\nu=0,1,-1} (Z_{\mu\nu}(\nabla\phi_\mu)(\nabla\phi_\nu) + Z'_{\mu\nu}(\nabla\theta_\mu)(\nabla\theta_\nu)), \tag{1}$$

where the phase stiffness matrix $Z_{\mu\nu}$ is real symmetric with both diagonal and off-diagonal components, and the fields ϕ_μ and θ_μ are dual to each other. To equation (1), we introduce sine-Gordon terms originating from generic fermion density–density interactions between left- and right-moving fermions corresponding to three spinless bands $\mu = 0, 1, -1$ (see figure 1, and equation (A1) in appendix A), which can be written as

$$\sum_\alpha g_\alpha \cos(2\sqrt{\pi}(\widetilde{a}_\mu^{(\alpha)}\phi_\mu)) + \sum_\beta G_\beta \cos(2\sqrt{\pi}(\widetilde{A}_\mu^{(\beta)}\theta_\mu)), \tag{2}$$

where the indices $\alpha = 1$–6, $\beta = 1$–3 and the coefficients of the sine-Gordon fields are given by

$$\begin{aligned}
\widetilde{a}^{(1)} &= (1, -1, 0)\\
\widetilde{a}^{(2)} &= (1, 0, -1)\\
\widetilde{a}^{(3)} &= (0, 1, -1)\\
\widetilde{a}^{(4)} &= (1, 1, 0)\\
\widetilde{a}^{(5)} &= (0, 1, 1)\\
\widetilde{a}^{(6)} &= (1, 0, 1)\\
\widetilde{A}^{(1)} &= (1, -1, 0)\\
\widetilde{A}^{(2)} &= (1, 0, -1)\\
\widetilde{A}^{(3)} &= (0, 1, -1).
\end{aligned}$$

We now diagonalize the stiffness matrix $Z_{\mu\nu}$ in the quadratic part of the bosonic Hamiltonian given in equation (1) by the following transformation to new bosonic fields $\widetilde{\phi_\mu}$ (given by [34])

$$\begin{pmatrix} \phi_1 \\ \phi_{-1} \\ \phi_0 \end{pmatrix} = \begin{pmatrix} \frac{1}{\sqrt{2}} & \frac{1}{\sqrt{6}} & \frac{1}{\sqrt{3}} \\ -\frac{1}{\sqrt{2}} & \frac{1}{\sqrt{6}} & \frac{1}{\sqrt{3}} \\ 0 & -\frac{2}{\sqrt{6}} & \frac{1}{\sqrt{3}} \end{pmatrix} \begin{pmatrix} \widetilde{\phi}_1 \\ \widetilde{\phi}_{-1} \\ \widetilde{\phi}_0 \end{pmatrix},$$

and likewise for the fields θ_μ. The 'noninteracting' part of the Hamiltonian, given by equation (1), can now be written as

$$H_0^{\mathrm{B}} = \frac{1}{2}\int \mathrm{d}x \sum_\mu v_\mu \left(K_\mu (\nabla \widetilde{\phi}_\mu)^2 + \frac{1}{K_\mu}(\nabla \widetilde{\theta}_\mu)^2 \right), \tag{3}$$

where $\mu = 0, 1, -1$ and the phase stiffness matrix, referred to as $\widehat{K}$, is diagonal. Note that our convention for K_μ differs from the one commonly used in the literature, where K_μ^{-1} takes the place of K_μ. There is a twofold degeneracy in the eigenvalues of the $\widehat{K}$-matrix ($v_1 K_1 = v_{-1} K_{-1} = v_\perp K_\perp$) in equation (3), which is a consequence of the C_3 rotational symmetry of the quadratic part of the Hamiltonian. Following the strategy of reference [6], we study the scaling of the quantities $K^\phi_{0,\perp} = v_{0,\perp} K_{0,\perp}$ and $K^\theta_{0,\perp} = \frac{v_{0,\perp}}{K_{0,\perp}}$, assuming an initial condition $v_{0,\pm 1} = 1$. We now define new rescaled fields $\widetilde{\psi}_{0,\pm 1} = \sqrt{K^\phi_{0,\perp}}\widetilde{\phi}_{0,\pm 1}$ and $\widetilde{\vartheta}_{0,\pm 1} = \sqrt{K^\theta_{0,\perp}}$ $\widetilde{\theta}_{0,\pm 1}$. Such a rescaling makes the stiffness matrix proportional to the identity matrix. During the RG process, we will find that small diagonal and off-diagonal corrections are introduced to the stiffness matrix, and it has a real symmetric form, which we once again denote by $Z_{\mu\nu}$.

In terms of the rotated and rescaled fields, the 'interacting' part of the bosonic Hamiltonian, in equation (2), has the form of coupled sine-Gordon terms

$$H_{\mathrm{int}}^{\mathrm{B}} = \sum_\alpha g_\alpha \cos(a_\mu^{(\alpha)} \widetilde{\psi}_\mu) + \sum_\beta G_\beta \cos(A_\mu^{(\beta)} \widetilde{\vartheta}_\mu), \tag{4}$$

where $\alpha = 1$–6, $\beta = 1$–3 and the coefficients of the sine-Gordon fields are now given by

$$\begin{aligned}
a^{(1)} &= \left(\frac{2\sqrt{2}\sqrt{\pi}}{\sqrt{K^\phi_\perp}}, \quad 0, \quad 0 \right),\\
a^{(2)} &= \left(\frac{\sqrt{2}\sqrt{\pi}}{\sqrt{K^\phi_\perp}}, \quad \frac{\sqrt{6}\sqrt{\pi}}{\sqrt{K^\phi_\perp}}, \quad 0 \right),\\
a^{(3)} &= \left(\frac{\sqrt{2}\sqrt{\pi}}{\sqrt{K^\phi_\perp}}, \quad -\frac{\sqrt{6}\sqrt{\pi}}{\sqrt{K^\phi_\perp}}, \quad 0 \right),\\
a^{(4)} &= \left(0, \quad \frac{4\sqrt{\pi}}{\sqrt{6}\sqrt{K^\phi_\perp}} \quad \frac{4\sqrt{\pi}}{\sqrt{3}\sqrt{K^\phi_0}} \right),
\end{aligned}$$

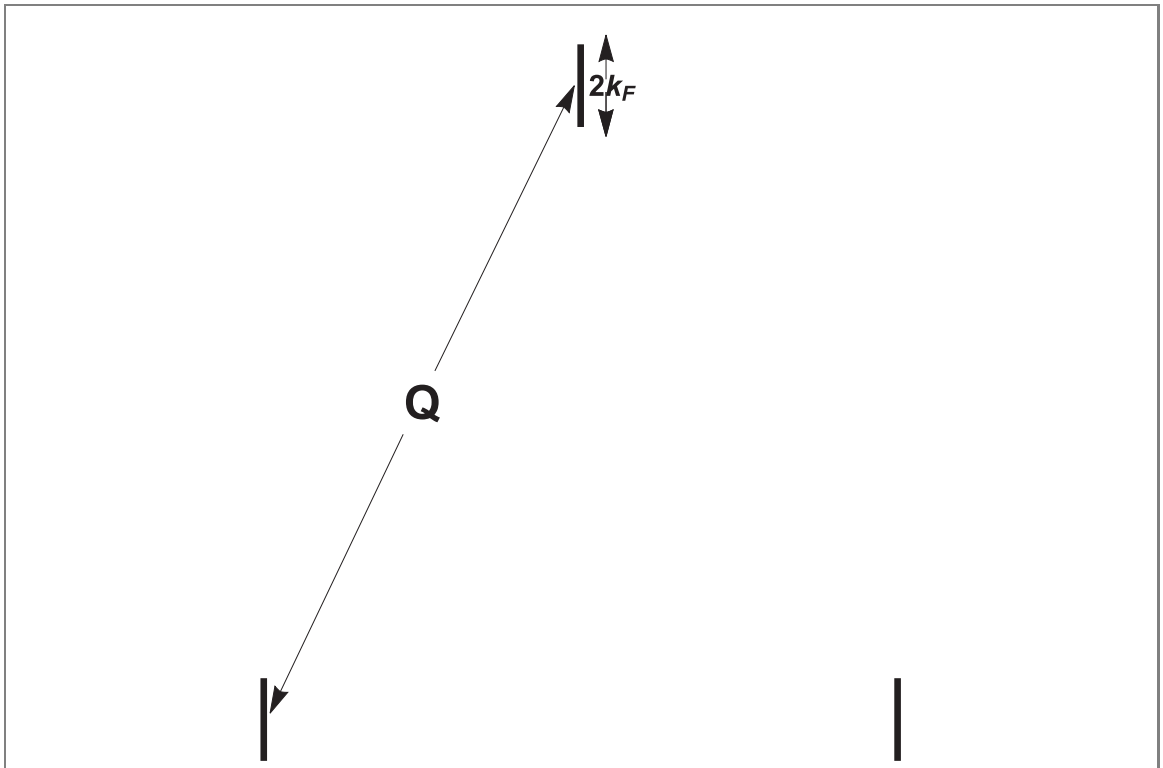

Figure 1. The figure shows three small Fermi pockets, with Fermi momentum k_F, separated by vectors Q in momentum space such that $Q \gg k_F$, which at sufficiently strong magnetic fields (quantum limit) behave effectively as spinless one-dimensional systems, illustrative of the situation being considered in the present analysis.

$$a^{(5)} = \left(\frac{\sqrt{2}\sqrt{\pi}}{\sqrt{K_\perp^\phi}}, \quad \frac{2\sqrt{\pi}}{\sqrt{6}\sqrt{K_\perp^\phi}}, \quad -\frac{4\sqrt{\pi}}{\sqrt{3}\sqrt{K_0^\phi}} \right),$$

$$a^{(6)} = \left(\frac{\sqrt{2}\sqrt{\pi}}{\sqrt{K_\perp^\phi}}, \quad -\frac{2\sqrt{\pi}}{\sqrt{6}\sqrt{K_\perp^\phi}}, \quad \frac{4\sqrt{\pi}}{\sqrt{3}\sqrt{K_0^\phi}} \right),$$

$$A^{(1)} = \left(\frac{2\sqrt{2}\sqrt{\pi}}{\sqrt{K_\perp^\theta}}, \quad 0, \quad 0 \right),$$

$$A^{(2)} = \left(\frac{\sqrt{2}\sqrt{\pi}}{\sqrt{K_\perp^\theta}}, \quad \frac{\sqrt{6}\sqrt{\pi}}{\sqrt{K_\perp^\theta}}, \quad 0 \right),$$

$$A^{(3)} = \left(\frac{\sqrt{2}\sqrt{\pi}}{\sqrt{K_\perp^\theta}}, \quad -\frac{\sqrt{6}\sqrt{\pi}}{\sqrt{K_\perp^\theta}}, \quad 0 \right),$$

In the rest of the paper, we perform a perturbative RG analysis on a bosonic Hamiltonian consisting of the quadratic part given by equation (3) and the sine-Gordon terms given in equation (4). In a generic strong correlation situation, the parameters $K^{\phi,\theta}$ in equation (3) may depart appreciably from unity [58–62] but this by itself does not lead to any instability of the Luttinger liquid. To induce electronic instabilities in the Luttinger liquid phase, we introduce physically relevant sine-Gordon perturbations that generally arise from interactions involving fermionic backscattering, as well as Umklapp scattering of pairs of fermions from one Fermi pocket to another, which is allowed in our model (see figure 1, and appendix A). Our emphasis on the parameter regime where $K^{\phi,\theta}$ is significantly different from unity is justified by our motivation of understanding electronic phase competition in the quantum limit in low-carrier density (and consequently strongly correlated) semimetals such as bismuth. The validity of the perturbative RG analysis we perform below requires the coupling constants g_α for the bosonic model to be small. During the RG procedure, the vectors $\widehat{a}$ and $\widehat{A}$, in general, rotate and stretch. The scaling dimensions for the interaction terms in equation (4) clearly depend on the values of the Luttinger parameters $K_0^{\phi,\theta}$ and $K_\perp^{\phi,\theta}$, and in our analysis, we only retain the most relevant interaction terms (with the smallest scaling dimensions), for the sake of simplicity.

3. Renormalization-group analysis

The RG analysis of the bosonic Hamiltonian, discussed in the previous section, follows the standard Wilsonian procedure of elimination of fast degrees of freedom, restoration of the cutoff, rescaling of the couplings and the renormalization of the fields. This gives rise to off-diagonal corrections in the stiffness matrices in the quadratic part, which then take the general real symmetric form $Z_{\mu\nu}$. To keep the Gaussian fixed point unchanged, we rotate the stiffness matrices $Z^{\theta,\phi}_{\mu\nu}$ so as to diagonalize them, which effectively rotates the bosonic fields. Note that the above rotation does not change the scaling dimensions of the sine-Gordon interaction terms. We then rescale the rotated fields using the eigenvalues of the diagonalized stiffness matrices $Z^{(\mu)}\delta_{\mu\nu}$, such that the latter become proportional to identity matrices. Now, in the new basis obtained after the rotation and the subsequent rescaling of the fields, we once again compute the one-loop corrections and the resulting changes in the diagonal and off-diagonal elements of the stiffness matrices (which are proportional to identity), and repeat the aforementioned steps throughout the RG process (see figure 2). We simplify our analysis by considering the anisotropic limits $K^{\phi}_{\perp} \gg K^{\phi}_{0}$ or $K^{\phi}_{0} \gg K^{\phi}_{\perp}$, which allows us to drop the sine-Gordon terms with the highest scaling dimensions in the interacting Hamiltonian in equation (4) in each of these limits. This necessarily means we are far from the noninteracting limit where $K^{\phi,\theta}_{0,\perp} \approx 1$, and our analysis corresponds to a strong coupling limit of the model. However, the formulation may be readily extended to the most general case.

3.1. Setting up the RG equations

Let us first discuss the results obtained by incorporating one-loop corrections to the matrices $Z^{\phi}_{\mu\nu}$ and $Z^{\theta}_{\mu\nu}$ in the two aforementioned anisotropic parameter regimes, $K^{\phi}_{\perp} \gg K^{\phi}_{0}$ and $K^{\phi}_{0} \gg K^{\phi}_{\perp}$. At any given stage of the RG, the matrix $Z^{\phi}_{\mu\nu}$, with the one-loop corrections incorporated, is given by

$$Z^{\phi} = \begin{pmatrix} \frac{1}{2} + \sum_{\alpha} \frac{g_{\alpha}^2\, dy}{16\pi}((a_1^{(\alpha)})^2 + (a_{-1}^{(\alpha)})^2)(a_1^{(\alpha)})^2 & \sum_{\alpha} \frac{g_{\alpha}^2\, dy}{16\pi}((a_1^{(\alpha)})^2 + (a_{-1}^{(\alpha)})^2)(a_1^{(\alpha)})(a_{-1}^{(\alpha)}) & 0 \\ \sum_{\alpha} \frac{g_{\alpha}^2\, dy}{16\pi}((a_1^{(\alpha)})^2 + (a_{-1}^{(\alpha)})^2)(a_1^{(\alpha)})(a_{-1}^{(\alpha)}) & \frac{1}{2} + \sum_{\alpha} \frac{g_{\alpha}^2\, dy}{16\pi}((a_1^{(\alpha)})^2 + (a_{-1}^{(\alpha)})^2)(a_{-1}^{(\alpha)})^2 & 0 \\ 0 & 0 & \frac{1}{2} \end{pmatrix}, \quad (5)$$

where g_{α} and $a_i^{(\alpha)}$ refer to the couplings and the coefficients of the sine-Gordon fields defined in equation (4), respectively, and $y \equiv \ln \Lambda$ is the RG flow parameter, where Λ refers to the cutoff scale in momentum space. The effect of $K^{\phi}_{0,\perp}$ on the RG equations is incorporated through the coefficients $a_i^{(\alpha)}$, as explained below. Note that the above matrix is block-diagonal—a consequence of the nature of the interaction terms and/or approximations employed in the parameter regimes considered in our analysis. In the limit where $K^{\phi}_{0} \ll K^{\phi}_{\perp}$, we find that we only need to retain the couplings $g_{\alpha}(\alpha = 1\text{–}3)$, based on their comparatively lower scaling dimensions (see equation (4)). In this case, we calculate one-loop corrections to the Z^{ϕ} matrices, of the form shown in equation (5) above, due to the terms g_1, g_2 and g_3 in the interaction Hamiltonian, and likewise, to the Z^{θ} matrices due to the terms G_1, G_2 and G_3. The corresponding matrix turns out to be block-diagonal, and independent of $K^{\theta,\phi}_{0}$ in this regime, due to the symmetry of the interaction terms. On the other hand, in the limit where $K^{\phi}_{\perp} \ll K^{\phi}_{0}$, only the couplings $g_{\alpha}(\alpha = 4\text{–}6)$ need to be retained in our analysis, based on their lower scaling dimensions. Then we obtain one-loop corrections to the Z^{ϕ} matrices arising only from the couplings g_4, g_5 and g_6 (and to the Z^{θ} matrices arising from the terms G_1, G_2 and G_3), which again reduce to the block-diagonal form given in equation (5) above with $\alpha = 4\text{–}6$ (the matrix is independent of $K^{\theta,\phi}_{0}$, this time due to the condition imposed on $K^{\theta,\phi}_{0}$ and $K^{\theta,\phi}_{\perp}$ in this parameter regime).

The next step in the RG procedure involves rotation of the stiffness matrices $Z_{\mu\nu}$ obtained above (meant to diagonalize them), followed by a rescaling of the fields (meant to restore the matrices to a form proportional to identity). These are finite rotations, which cannot be accounted for in the RG flow equations. In our approach, we are always in the rotating frame, where these large rotations are absent, and only small incremental changes to the components along the field directions need to be tracked. These amount to slow changes in the orientation and length, in the rotating frame, upon scaling. Now, the rotation and rescaling of the fields in the sine-Gordon terms effectively results in a rotation and rescaling of the coefficients of the fields $(a_i^{(\alpha)}, A_j^{(\beta)})$. If the eigenvalues of the matrix $Z_{\mu\nu}$ in equation (5) above are denoted by z_1, z_{-1} and z_0, at any given stage of the RG flow, the coefficients of the fields in the cosine terms evolve in the manner $a_i^{(\alpha)} \to \frac{(Ra^{(\alpha)})_i}{\sqrt{z_i}}$, where R is the rotation which diagonalizes the matrix $Z_{\mu\nu}$. We continue

to denote the interaction terms as $g_\alpha \cos[\widehat{a}_i^{(\alpha)}\widetilde{\psi}_i]$ and $G_\beta \cos[\widehat{A}_j^{(\beta)}\widetilde{\vartheta}_j]$, and track the scaling equations for the coefficients $a_i^{(\alpha)}, A_j^{(\beta)}$, along with the couplings g_α, G_β.

Proceeding in incremental steps, the RG equations for the coefficients $a_1^{(1)}$ and $a_{-1}^{(1)}$ (corresponding to the coupling g_1) due to the rescaling process described above, are given by

$$\frac{\mathrm{d}a_1^{(1)}}{\mathrm{d}y} = -a_1^{(1)}\Lambda_1$$
$$\frac{\mathrm{d}a_{-1}^{(1)}}{\mathrm{d}y} = -a_{-1}^{(1)}\Lambda_{-1}, \tag{6}$$

where $z_1 = 1/2 + \Lambda_1 \mathrm{d}y$ and $z_{-1} = 1/2 + \Lambda_{-1}\,\mathrm{d}y$ are the eigenvalues of the matrix $Z_{\mu\nu}$ at a given step of the RG, described previously, with $\Lambda_1(a_i^{(\alpha)}, g_\alpha)$ and $\Lambda_{-1}(a_i^{(\alpha)}, g_\alpha)$ ($\alpha = 1, 2, 3$, $i = 1, -1$ in this case) depending upon all the coupling constants and the coefficients of all the fields in the sine-Gordon terms, as evident from equation (5) above (see appendix B for the explicit expressions of Λ_1 and Λ_{-1}). The initial conditions for $a_i^{(\alpha)}$ depend on $K_\perp^\phi$ as well as the initial couplings g_α. The leading corrections are quadratic in the coupling constants. The RG flow equations for the rest of the components $a_i^{(\alpha)}$ also behave in the same way. The tree-level contributions to the RG flows for the sine-Gordon couplings g_α are obtained in terms of the scaling dimensions of the respective sine-Gordon terms. The RG equations for the couplings $g_\alpha, \alpha = 1$–3 are

$$\frac{\mathrm{d}g_1}{\mathrm{d}y} = g_1\,(2 - \frac{1}{4\pi}((a_1^{(1)})^2 + (a_{-1}^{(1)})^2),$$
$$\frac{\mathrm{d}g_2}{\mathrm{d}y} = g_2\,(2 - \frac{1}{4\pi}((a_1^{(2)})^2 + (a_{-1}^{(2)})^2),$$
$$\frac{\mathrm{d}g_3}{\mathrm{d}y} = g_3\,(2 - \frac{1}{4\pi}((a_1^{(3)})^2 + (a_{-1}^{(3)})^2). \tag{7}$$

The RG equations for the rest of the couplings $g_\alpha(\alpha = 4$–$6)$ as well as $G_\alpha(\alpha = 1$–$3)$ have a similar form as equation (7). It is clear from equation (6) that there is an interplay between the different couplings even at the tree-level order in equation (7).

One-loop corrections to the RG equations: in equation (7) above, we have neglected the $O(g^2)$ one-loop (or operator product expansion (OPE)) contributions to the renormalization of the coupling constants g_α, which are perturbatively smaller than the leading tree-level term. OPE terms are important in parameter regimes they are perturbatively comparable to the tree-level term. However, if the initial values of the sine-Gordon couplings are small, and the initial stiffnesses $K^{\phi,\theta}$ are appreciably different from unity (as is the case in our analysis), we found that the RG equations with or without the one-loop corrections generally give very similar solutions, and therefore, we only consider the tree-level contributions in our analysis. If the initial scaling dimensions of the interaction terms are close to two (i.e. the tree-level contribution is small), or the bare values of the couplings are not sufficiently small (so that the one-loop and tree-level terms are comparable), then the one-loop terms also need to be taken into account. This requires a separate, more detailed study and is not attempted in the present work.

We solve the coupled differential equations in equation (6) (and its counterparts for the rest of the coefficients $a_i^{(\alpha)}$) and equation (7) numerically and obtain the fixed-point values for the various couplings g_α and the coefficients $a_i^{(\alpha)}$, applicable for the different parameter regimes considered. We consider weak repulsive interactions in every channel, and study the nature of the RG flows as a function of the initial conditions on the couplings g_α and the value of the Luttinger liquid parameter $K_\perp^{\phi,\theta}$, which enters in the initial conditions of $a_i^{(\alpha)}$ and $A_j^{(\beta)}$. We find that the couplings g_α either diverge or flow to zero in the course of the RG flow (see figure 3). From equation (6) above, it is clear that the coefficients $a_i^{(\alpha)}$ of the different bosonic fields rescale differently. In the course of the RG flow, these either decay to zero, or flow to a constant value.

4. Phase diagram and critical behaviour

The order parameters considered in our analysis are fermionic bilinears characterized by chirality and band indices, belonging to two broad classes, namely the p–h channel (density wave),

$$\mathrm{Re}[O_{\mathrm{ph}}^{i0}] \propto \sum_{mm'} \lambda^i_{mm'} \psi^\dagger_{\mathrm{R}m} \psi_{\mathrm{L}m'} + \mathrm{h.c}, \tag{8}$$

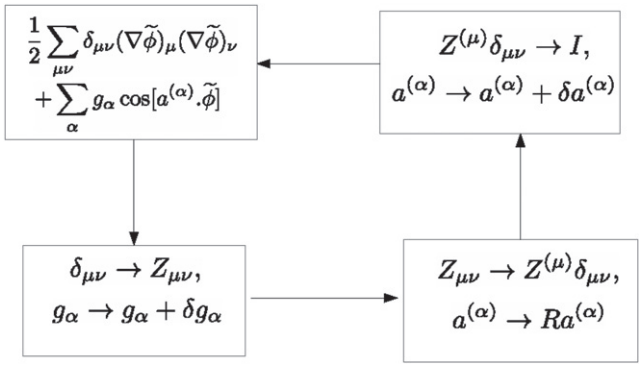

Figure 2. The figure shows a schematic illustration of our RG procedure. The stiffness matrix, which is initially diagonal, develops off-diagonal corrections in the course of the RG flow and takes the general form $Z_{\mu\nu}$. This matrix is diagonalized, which leads to a rotation R of the coefficients $a^{(\alpha)}$ of the sine-Gordon interaction terms. The diagonal elements are then absorbed in the respective sine-Gordon fields, which brings the stiffness matrix back to unity, and leads to a rescaling of the rotated coefficients $a^{(\alpha)}$.

Table 1. Table showing electronic phases corresponding to each of the order parameters considered in our analysis. Here particle–particle (p–p) refers to superconductivity, while particle–hole (p–h) refers to density wave orders. In the fermionic picture involving three spinless bands, interband pairing between different pairs of bands in the p–h channel leads to bond order (denoted by BO) while the corresponding pairing in the p–p channel leads to a finite-momentum pairing (denoted by FFLO) state with the wavevector Q, equal to the separation between two small Fermi pockets in momentum space. Intraband pairing can correspond to a situation with different phases on different Fermi pockets and lead to uniform charge density wave (denoted by UCDW) or nematic d-density wave order (denoted by NCDW) in the p–h channel, and s-wave or nematic d-wave superconductivity in the p–p channel. In the case where these different order parameters are degenerate, a combination of them which is chiral in nature gives rise to the lowest energy configuration. In such a situation, a chiral d-density wave (denoted by cCDW) or chiral d-wave superconductivity can be realized.

Type of order		Order parameter	Name of order
Interband	p–p	$O^{10}_{pp}, O^{40}_{pp}, O^{60}_{pp}$	FFLO (wavevector Q)
		$O^{20}_{pp}, O^{50}_{pp}, O^{70}_{pp}$	FFLO (wavevector Q)
	p–h	$O^{10}_{ph}, O^{40}_{ph}, O^{60}_{ph}$	Bond order (BO) (wavevector Q)
		$O^{20}_{ph}, O^{50}_{ph}, O^{70}_{ph}$	Bond order (BO) (wavevector Q)
Intraband	p–p	$O^{00}_{pp}, O^{30}_{pp}, O^{80}_{pp}$	s-wave (SW), nematic d-wave, chiral d-wave
	p–h	$O^{00}_{ph}, O^{30}_{ph}, O^{80}_{ph}$	Uniform(U) CDW, nematic (N) d-CDW, chiral (c) d-CDW

and the p–p channel (superconductor),

$$\mathrm{Re}[O^{i0}_{pp}] \propto \sum_{mm'} \lambda^i_{mm'} \psi^\dagger_{Rm} \psi^\dagger_{Lm'} + \mathrm{h.c}, \tag{9}$$

where $\lambda^i (i = 1 \ldots 8)$ correspond to the Gell–Mann matrices (see appendix C for details), λ^0 denotes the 3×3 unit matrix, and $\psi_{pm}(\psi^\dagger_{pm})$ is the electron annihilation (creation) operator with chirality p and band m. We follow the convention used by reference [34]; however, in both the equations (8) and (9), no spin indices are present. The order parameters in equations (8) and (9 above are expressed in terms of the bosonic fields, using the usual bosonization prescription. A total of eighteen order parameters can be thus constructed in the p–h and p–p channels in the spinless case (see appendix C for expressions of the order parameters in terms of the bosonic fields). Similarly, one can also consider some equal-chirality pairings, which have to be treated on a case-by-case basis.

We now discuss the physical meaning of the electronic phases corresponding to the above order parameters. In the anisotropic strong coupling regime that we study (where the initial $K^\phi_\perp$ value is often far from unity and the initial g_α are generically unequal), the phases that are obtained are typically associated with the breaking of permutation between different flavours of bosonic fields or bond permutation symmetries corresponding to pairs of flavours. In the fermionic picture, comprising three spinless bands (see appendix A), interband pairing in the p–h channel corresponds to a bond-ordered (BO) phase, while in the p–p channel it gives rise to superconductivity at a finite wavevector (Fulde–Ferrell–Larkin–Ovchinnikov or FFLO phase) equal to the separation between two small Fermi pockets in momentum space, Q. Likewise, the intraband order parameters correspond to linear combinations of the fermionic bilinears on the three different pockets. One of them is a symmetric linear combination ($s-$wave, denoted

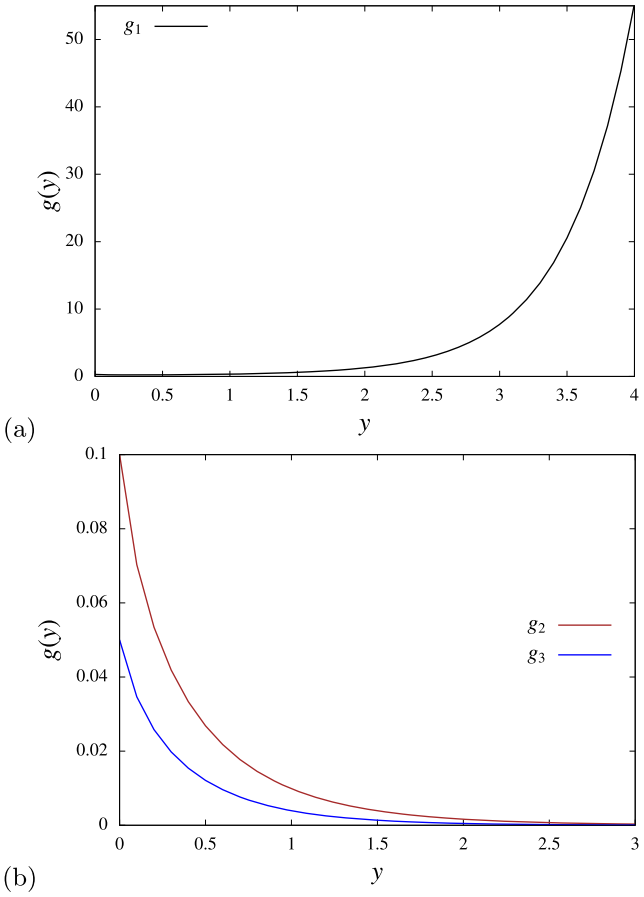

Figure 3. The figure shows the RG flows for the couplings g_1, g_2 and g_3 for the Luttinger parameter $K_\perp^\phi = 0.3$ and initial conditions $g_1^0 = 0.3$, $g_2^0 = 0.1$, $g_3^0 = 0.05$, for illustration. While g_1 grows monotonously (see (a)) under these conditions, g_2 and g_3 show a decline (see (b)). In general, any one or more of the couplings g_α may diverge, depending on the initial conditions chosen.

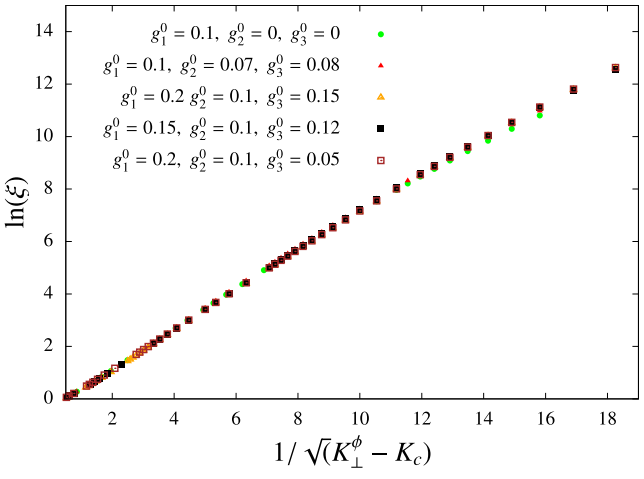

Figure 4. The figure shows a scaling collapse plot of the RG flow parameter $y \sim \ln[\xi]$ (where ξ is the correlation length) as a function of $\frac{1}{\sqrt{K_\perp^\phi - K_c}}$. K_c denotes the critical value of the Luttinger liquid parameter $K_\perp^\phi$, where the system undergoes a phase transition. The plot shows results for five different sets of initial conditions on the interactions, with one or more of the couplings g_α taking non-zero values initially, and indicates that the phase transitions occurring in this system are continuous in nature and belong to the BKT universality class.

by SW) while the other two are nematic, corresponding to angular momentum $l = 2$ (d-wave order). If we ascribe the angular positions of the three fermionic patches in momentum space as $\delta = 0$, $\delta = 2\pi/3$ and $\delta = 4\pi/3$, the phases of the order parameters, corresponding to the three patches, go either as $\cos(2\delta)$ or $\sin(2\delta)$, both of the d-wave type. It is also possible to have chiral orders, with phases going as $\exp(\pm i\delta)$, as a linear combination of nematic orders. These linear combinations are not unique, and depending on the initial conditions, the actual order parameter may be some combination of these. Intraband pairing in the

p–h channel has an ordering wavevector $2k_F$, much less than Q, and is generally incommensurate (see figure 1). Depending on the initial conditions, the CDW (charge density wave) order could involve a linear combination of the CDW orders on the three different patches. If C_3 symmetry is not broken, then the orders may have s-wave (uniform CDW, denoted by UCDW), or a doubly degenerate d-wave symmetry (d-density wave). As was the case for superconductivity, the d-density wave order can be either nematic (denoted by NCDW) or chiral type (denoted by cCDW). The order parameters corresponding to different types of order are listed in table 1.

To study the dominant electronic orders, we introduce, in the disordered phase, test vertices corresponding to various order parameter fluctuations and determine how they grow or shrink upon scaling. The evolution of any particular order parameter is governed by a certain combination of couplings, and the one with the smallest scaling dimension, such that the divergence is strongest upon scaling, is the dominant order. Those order parameters that initially have a large scaling dimension do not grow under scaling and correspond to short-range order. While at leading order in perturbation this is completely equivalent to the usual approach of studying the long-range ordering of the fields which correspond to the most divergent couplings, it has the advantage that it allows us to study the competition between different order parameters, by taking into account the corrections to the scaling dimensions of the bosonized order parameters to leading order, $O(g)$ in the couplings. These terms sometimes lead to shifts in the scaling dimensions of order parameters that have identical RG equations at the tree-level order, resulting in the lifting of degeneracies, with one of them becoming long-range ordered and the other short-range ordered (see appendix C). The behaviour of the couplings g_α and the corresponding coefficients of the fields $a_i^{(\alpha)}$ near the fixed point of the RG, for a given set of initial conditions, play a crucial role in deciding the nature of the dominant electronic orders. In some cases, we find that none of the order parameters we studied grows under RG, implying the absence of any quasi-long range ordered state despite the presence of interactions. Such situations also come up in the context of floating phases in coupled sine-Gordon models. Another advantage of our method is that it not only gives us the dominant order parameters, but also yields the scaling dimension at the fixed point, which is essentially the exponent of power law correlations of the order parameter fields in the quasi-long range ordered state.

The nature of the phase transitions is studied using a numerical scaling analysis. The scaling of the correlation length ξ at the critical point is determined by identifying the characteristic scale y where the couplings $g_\alpha(y)$ cross a designated value $\gtrsim 1$. We obtain continuous transitions as a function of $K_\perp^\phi$, belonging to the BKT universality class, which is confirmed by demonstrating the universal BKT scaling collapse for the behaviour of the correlation length close to the critical point (see figure 4). Note that the critical value K_c of the Luttinger parameter $K_\perp^\phi$ is different for different initial conditions on the couplings g_α, as shown in figure 4, each of which give rise to the same critical behaviour.

4.1. Phase diagram

We classify the nature of the dominant orders in different parameter regimes depending upon the relative sizes of $K_\perp^\phi$ and K_0^ϕ, considering, broadly, the regimes $K_0^\phi \gg K_\perp^\phi$ and $K_\perp^\phi \gg K_0^\phi$. Within each of these classes, we further examine situations with either $K_0^\phi \gg 1$ or $K_0^\phi \ll 1$. The case with $K_0^\phi \sim 1$, involving a competition between different types of orders, depending upon the initial conditions, requires a more detailed study, and has not been addressed here. In the regime where $K_0^\phi \gg K_\perp^\phi$ and $K_0^\phi \ll 1$, the dominant instabilities are found in the intraband p–p channel, based on the smaller scaling dimensions of the corresponding bosonized expressions for the order parameters. Similarly, in the regime where $K_\perp^\phi \gg K_0^\phi$ and $K_0^\phi \gg 1$, the dominant instabilities are found in the intraband p–h channel. Note that in these two parameter regimes, $K_\perp^\phi$ is automatically constrained to be numerically very small or very large. We now consider the remaining two cases, which allow us to tune $K_\perp^\phi$ over a wide range of values, giving rise to both intraband and interband orders. We find that for $K_0^\phi \gg K_\perp^\phi$ and $K_0^\phi \gg 1$, the p–h orders are more relevant than the p–p orders, due to smaller scaling dimensions of the corresponding order parameters, and for $K_\perp^\phi \gg K_0^\phi$ and $K_0^\phi \ll 1$, the p–p orders are likewise found to be more important. Within the regimes considered by us, the phase diagram is affected primarily by two factors: the magnitude of the Luttinger liquid parameter $K_\perp^\phi$ and the set of initial conditions considered for the interactions g_α. Note that we do not need to explicitly consider numerical values for $K_0^{\phi,\theta}$ in our analysis, since we drop the terms involving these parameters due to the constraints imposed upon them.

Below we discuss the salient features of the phase diagram for the aforementioned two parameter regimes, $K_0^\phi \gg K_\perp^\phi$ and $K_0^\phi \gg 1$, or $K_0^\phi \ll K_\perp^\phi$ and $K_0^\phi \ll 1$, each corresponding to a range of values of $K_\perp^\phi$. Since $K_\perp^\theta$ is inversely related to $K_\perp^\phi$ in our model, the latter does not constitute an independent parameter in the phase diagram.

$K_\perp^\phi \ll 1$: in this regime, for $K_0^\phi \ll K_\perp^\phi$ and $K_0^\phi \ll 1$, the intraband p–p orders (SW, nematic, chiral) are found to be more relevant, whereas for $K_0^\phi \gg K_\perp^\phi$ and $K_0^\phi \gg 1$, no electronic orders are present

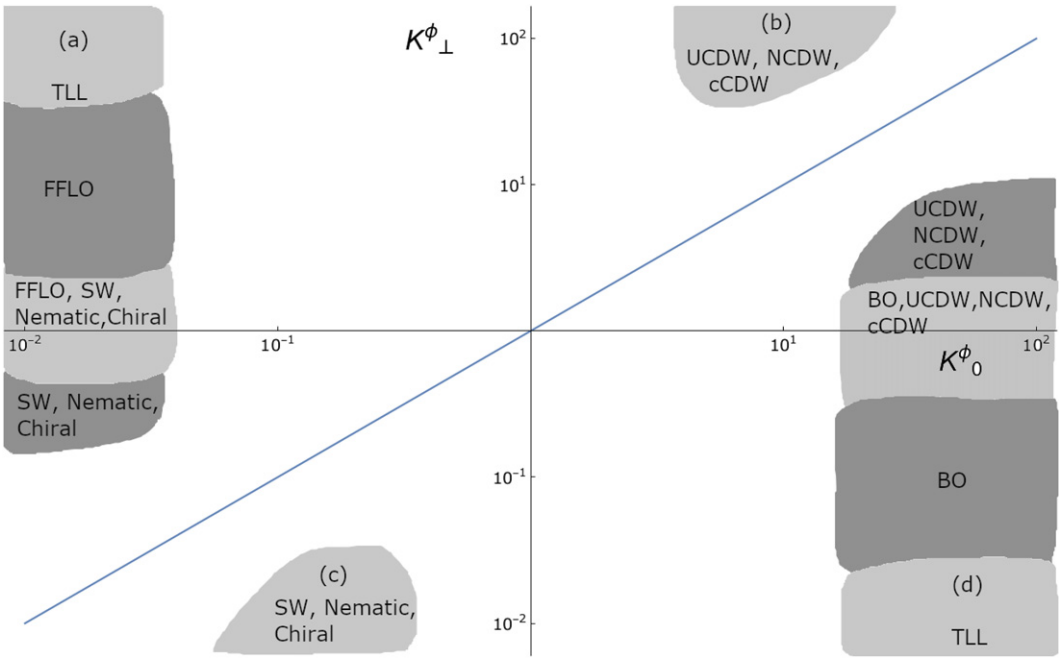

Figure 5. The figure shows the phase diagram for a system of three coupled spinless Luttinger liquids as a function of $K^{\phi}_{\perp}$, considering the parameter regimes (a) $K^{\phi}_{\perp} \gg K^{\phi}_{0}$ and $K^{\phi}_{0} \ll 1$, where only p–p orders are considered due to the smaller scaling dimensions of the corresponding order parameters, (b) $K^{\phi}_{\perp} \gg K^{\phi}_{0}$ and $K^{\phi}_{0} \gg 1$, where the dominant instabilities belong to the intraband p–h channel, (c) $K^{\phi}_{0} \gg K^{\phi}_{\perp}$ and $K^{\phi}_{0} \ll 1$ where the dominant instabilities occur in the intraband p–p channel, and (d) $K^{\phi}_{0} \gg K^{\phi}_{\perp}$ and $K^{\phi}_{0} \gg 1$, where only p–h orders are considered in our analysis, due to smaller scaling dimensions of the corresponding terms. In cases (a) and (d), we can tune $K^{\phi}_{\perp}$ over a large range of values, and for $K^{\phi}_{\perp} \sim 1$, various interband and intraband orders compete with one another, the winner being determined by the initial conditions on the interactions. Note that our results are not reliable for $K^{\phi}_{\perp} = 1$ in regime (a), where the one-loop corrections must be taken into account. The orders indicated in the figure have been denoted in the paper as SW for *s*-wave, FFLO for finite-momentum pairing, UCDW as a CDW order with s-wave symmetry, NCDW as nematic *d*-density wave, cCDW as chiral *d*-density wave and BO as bond order, and TLL refers to the Tomonaga Luttinger liquid. The various shaded (light and dark grey) portions of the phase diagram demarcate the parameter regimes which can be understood from our analysis. The different shaded regions correspond to various possible instabilities of the initial gapless Luttinger liquid phase, in the presence of perturbative sine-Gordon terms, for a given ratio $K^{\phi}_{\perp}/K^{\phi}_{0}$ and given initial values for the coupling constants. The boundaries of different types of phases are flexible in nature, and can change depending on the initial conditions chosen for the couplings. In particular, the above phase diagram corresponds to the initial conditions $g^{0}_{1} = 0.09, g^{0}_{2} = 0.08, g^{0}_{3} = 0.07, g^{0}_{4} = 0.09, g^{0}_{5} = 0.08, g^{0}_{6} = 0.07, G^{0}_{1} = 0.09, G^{0}_{2} = 0.08, G^{0}_{3} = 0.07$.

(corresponding to the Tomonaga Luttinger liquid phase, denoted by TLL) when we consider extremely small values of $K^{\phi}_{\perp}$, and for larger values of $K^{\phi}_{\perp}$, a particular pair of interband p–h orders (BO) dominates, depending upon the initial conditions being considered for the interactions.

$K^{\phi}_{\perp} \sim 1$: for $K^{\phi}_{\perp} \sim 1$, various intraband and interband p–p (FFLO, SW, nematic, chiral) orders compete with each other in the regime $K^{\phi}_{0} \ll K^{\phi}_{\perp}$ and $K^{\phi}_{0} \ll 1$, and likewise, various p–h (UCDW, NCDW, cCDW, BO) orders compete with each other in the regime $K^{\phi}_{0} \gg K^{\phi}_{\perp}$ and $K^{\phi}_{0} \gg 1$, and it is in this part of the phase diagram that the winning phases are dependent most sensitively on the initial conditions chosen for the interactions. However, at $K^{\phi}_{\perp} = 1$ for $K^{\phi}_{0} \ll K^{\phi}_{\perp}$, or very close to this point, the one-loop corrections should be taken into account, and our analysis in this regime requires further work.

$K^{\phi}_{\perp} \gg 1$: in this case, for $K^{\phi}_{0} \ll K^{\phi}_{\perp}$ and $K^{\phi}_{0} \ll 1$, a particular pair of interband p–p orders (FFLO) is found to dominate, depending on the initial conditions chosen for the interactions, and no order is found to be present when we consider extremely large values of $K^{\phi}_{\perp}$, whereas for $K^{\phi}_{0} \gg K^{\phi}_{\perp}$ and $K^{\phi}_{0} \gg 1$, the intraband p–h orders (UCDW, NCDW, cCDW) are found to be more relevant.

The types of electronic orders occurring in different parameter regimes, considered in our analysis, are schematically shown in figure 5, where the different shades of grey demarcate various possible ordered phases, and the boundaries between these different types of ordered phases are obtained by searching for the most dominant orders, which diverge the fastest under the RG, in a given parameter regime for $(K^{\phi}_{\perp}, K^{\phi}_{0})$, and for a given set of initial conditions on the couplings.

5. Discussion and conclusions

In summary, we have studied competing electronic phases and phase transitions in a system of three coupled spinless Luttinger liquids, using a perturbative RG analysis of the bosonic model, that takes into

account off-diagonal contributions arising from one-loop corrections to the stiffness matrices. This is done by introducing a series of rotations and rescalings of the fields (or equivalently, the coefficients of different fields in the sine-Gordon interaction terms) in the course of the RG flow. To determine the most dominant electronic orders, we introduce, in the disordered phase, test vertices corresponding to various order parameter fluctuations and study their evolution under the RG. The overall nature of the winning orders in different parameter regimes is governed by the RG flows of the couplings, as well as those of the coefficients of the fields in the sine-Gordon terms. Notably, for a range of values of the Luttinger liquid parameter $K_\perp^\phi$, which depart appreciably from the noninteracting limit $K_\perp^\phi = 1$, interband orders involving any one pair of fermionic bands (or equivalently, one pair of bosonic fields) are found to be dominant, the specific pair being determined by the initial conditions for the couplings. This is an example of valley symmetry breaking (to be discussed below in the context of systems with multiple small Fermi pockets), manifested as symmetry breaking between different bosonic flavours. At $K_\perp^\phi = 1$ for $K_\perp^\phi \gg K_0^\phi$, one-loop corrections to the RG equations must be taken into account, and this aspect of our analysis requires further work. In the regions where intraband orders involving a single fermionic band (or equivalently, one bosonic flavour) are the most relevant, they can be chiral in nature. For simplicity of analysis, we have considered the strong correlation regimes of $K_0^\phi \gg 1$ or $K_0^\phi \ll 1$, and the more involved case of $K_0^\phi \sim 1$ has not been discussed, where the p–p and p–h channels compete with each other and the results are likely to be sensitive to the initial conditions considered. This will be taken up in a future work. We also determine the nature of the phase transitions as a function of the Luttinger parameter $K_\perp^\phi$ as well as the initial conditions on the interactions g_α using a numerical scaling analysis. The system features continuous transitions belonging to the BKT universality class.

From an experimental point of view, our analysis is expected to be relevant for studying electronic interaction effects in semimetals with three small Fermi pockets under conditions of high magnetic fields such that the bands are effectively in the quantum limit, and may be regarded as one-dimensional. Examples include bismuth and graphite intercalation compounds. For bismuth, when the magnetic field is aligned along the highest symmetry axis (the trigonal axis), a field of 9 T allows one to attain the quantum limit, putting carriers in their lowest Landau level [46]. In this situation, Coulomb interaction effects play an important role in determining the electronic phase. The presence of anomalous features in the magnetization [39] and the Nernst response [36] of bismuth at high fields, beyond the quantum limit, points towards the importance of examining possible electronic instabilities due to interaction effects in this regime. Furthermore, there has been experimental evidence for valley symmetry breaking at high magnetic fields in bismuth [38]. We expect our technique to be useful for theoretically describing such a system, incorporating the known experimental features known from experiment (see appendix D for an estimate of the relevant couplings for a system like bismuth in the presence of a large applied magnetic field). In graphite intercalates, the Fermi level often naturally lies in the vicinity of the M-points in the Brillouin zone, which gives rise to another system with three small Fermi pockets, where the behaviour of the system beyond the quantum limit may be accessible through our analysis.

In the present work, we have not studied the case where $K_0^\phi \sim K_\perp^\phi$, with the rotations being in general O(3) matrices. The rotation matrices in that case are non-abelian and it would interesting to see if this gives qualitatively new insights into the problem. In this regime, we also have the possibility of an additional Ising-type symmetry breaking due to the symmetry between the $\widetilde{\theta}$ and $\widetilde{\phi}$ fields when $K_\perp^\phi = K_0^\phi = 1$, which has not been considered in this paper. We hope to study the implications of our approach for the spinful three-band case, and compare our results with reference [34], where the rotations of the matrices $Z_{\mu\nu}$ were not taken into account in the RG analysis. We would also like to consider the case of special fillings where intraband Umklapp scattering terms are possible. At first sight, these terms have higher scaling dimensions than the interactions considered by us, and so, at the tree level, they are not relevant. However, more work needs to be done to see the effect they have on the conclusions of this paper.

Acknowledgments

SK acknowledges funding support from the Canada First Research Excellence Fund (CFREF), and from the Dirac fellowship sponsored by the National High Magnetic Field Laboratory (NHMFL).

Data availability statement

No new data were created or analysed in this study.

Appendix A. Fermionic Hamiltonian

In our analysis, we consider a bosonized Luttinger liquid Hamiltonian with three flavours of Bose fields, which is perturbed by sine-Gordon terms originating from generic fermion density–density interactions, between left- and right-moving fermions. The three spinless fermionic fields are expanded in the vicinity of the two Fermi points. We are interested in situations that physically correspond to partially filled bands, so that Umklapp scattering between the two Fermi points for a given band is not relevant. However, since we would like our model to be relevant for systems with multiple nested Fermi pockets with a nesting vector equal to half a reciprocal lattice vector (such as in the case of bismuth), we do allow the possibility of two-particle Umklapp scattering between pockets, such that the total momentum transferred corresponds to a reciprocal lattice vector.

With these assumptions, the fermionic interactions take the following form,

$$\begin{aligned} H_{\rm int} = \sum_{p,m} (&g_1^{(1)} \psi^\dagger_{pm} \psi^\dagger_{\bar{p}\bar{m}} \psi_{pm} \psi_{\bar{p}\bar{m}} + g_1^{(2)} \psi^\dagger_{pm} \psi^\dagger_{\bar{p}\bar{m}} \psi_{\bar{p}m} \psi_{p\bar{m}} \\ &+ g_1^{(3)} \psi^\dagger_{pm} \psi^\dagger_{p\bar{m}} \psi_{\bar{p}m} \psi_{\bar{p}\bar{m}} + g_1^{(4)} \psi^\dagger_{pm} \psi^\dagger_{p\bar{m}} \psi_{pm} \psi_{p\bar{m}} \\ &+ g_2^{(1)} \psi^\dagger_{pm} \psi^\dagger_{\bar{p}\bar{m}} \psi_{p\bar{m}} \psi_{\bar{p}m} + g_2^{(2)} \psi^\dagger_{pm} \psi^\dagger_{\bar{p}\bar{m}} \psi_{\bar{p}\bar{m}} \psi_{pm} \\ &+ g_2^{(3)} \psi^\dagger_{pm} \psi^\dagger_{p\bar{m}} \psi_{\bar{p}\bar{m}} \psi_{\bar{p}m} + g_2^{(4)} \psi^\dagger_{pm} \psi^\dagger_{p\bar{m}} \psi_{p\bar{m}} \psi_{pm} \\ &+ g_3^{(1)} \psi^\dagger_{pm} \psi^\dagger_{\bar{p}m} \psi_{p\bar{m}} \psi_{\bar{p}\bar{m}} + g_3^{(2)} \psi^\dagger_{pm} \psi^\dagger_{\bar{p}m} \psi_{\bar{p}\bar{m}} \psi_{p\bar{m}} \\ &+ g_3^{(3)} \psi^\dagger_{pm} \psi^\dagger_{pm} \psi_{\bar{p}\bar{m}} \psi_{\bar{p}\bar{m}} + g_3^{(4)} \psi^\dagger_{pm} \psi^\dagger_{pm} \psi_{p\bar{m}} \psi_{p\bar{m}} \\ &+ g_4^{(1)} \psi^\dagger_{pm} \psi^\dagger_{\bar{p}m} \psi_{pm} \psi_{\bar{p}m} + g_4^{(2)} \psi^\dagger_{pm} \psi^\dagger_{\bar{p}m} \psi_{\bar{p}m} \psi_{pm} \\ &+ g_4^{(4)} \psi^\dagger_{pm} \psi^\dagger_{pm} \psi_{pm} \psi_{pm}) , \end{aligned} \tag{A1}$$

where $p = 1(-1)$ refers to right (left) moving fermions, and $m = 0, 1, -1$ denotes the bands and $\overline{m} \neq m$. The three bands are regarded as identical, for simplicity. The above model is C_3 symmetric under the permutation of the three bands. To study the low-energy behavior, we shall utilize the standard bosonization technique to analyze the continuum fermion model. We now bosonize the fermionic model using the abelian bosonization prescription,

$$\psi_{pm} = \frac{\eta_{pm}}{\sqrt{2\pi a}} \exp[\mathrm{i}pk_{\rm Fm}x] \exp[-\mathrm{i}p\sqrt{\pi}\varphi_{pm}], \tag{A2}$$

where $k_{\rm Fm}$ is the Fermi momentum for band m, a is a cutoff of the order of the lattice constant, and $p = 1(-1)$ stands for the R(L) branch. The Majorana Klein factors $\eta_{\rm R/Lm}$ satisfy

$$\{\eta_{\rm Rm}, \eta_{\rm Rm'}\} = 2\delta_{mm'}$$

$$\{\eta_{\rm Lm}, \eta_{\rm Lm'}\} = 2\delta_{mm'}$$

$$\{\eta_{\rm Rm}, \eta_{\rm Lm'}\} = 0.$$

We adopt the following convention for the Klein factors, following reference [34],

$$\eta_{mp}\eta_{\overline{m}p} = \eta_{0p}\eta_{mp} = \mathrm{i}mp,$$

$$\eta_{mp}\eta_{m\bar{p}} = \eta_{0p}\eta_{0\bar{p}} = \mathrm{i}p,$$

$$\eta_{mp}\eta_{\overline{m}\bar{p}} = \eta_{0p}\eta_{m\bar{p}} = \mathrm{i}m,$$

where $p, m = \pm 1$. The chiral fields φ_{pm} can be written in terms of nonchiral fields ϕ_m and θ_m as $\varphi_{pm} = \phi_m - p\theta_m$, and their gradients are proportional to the fermionic density and current operators, respectively, i.e.,

$$\begin{aligned} \nabla\phi_m &\propto \psi^\dagger_{\rm Rm}\psi_{\rm Rm} + \psi^\dagger_{\rm Lm}\psi_{\rm Lm} \\ \nabla\theta_m &\propto \psi^\dagger_{\rm Rm}\psi_{\rm Rm} - \psi^\dagger_{\rm Lm}\psi_{\rm Lm}. \end{aligned} \tag{A3}$$

Appendix B. Details of the RG equations

In the RG equations in equation (6) the expressions for Λ_1 and Λ_{-1} are given by

$$\Lambda_{\pm 1} = \frac{1}{32\pi}\Big((a_1^2+a_{-1}^2)^2 g_1^2 + (b_1^2+b_{-1}^2)^2 g_2^2 + (c_1^2+c_{-1}^2)^2 g_3^2 \pm (a_1^8 g_1^4 + 4a_1^6 a_{-1}^2 g_1^4 + 4a_1^2 a_{-1}^6 g_1^4 + a_{-1}^8 g_1^4$$
$$+z(b_1^2+b_{-1}^2)^4 g_2^4 + 2(b_1^2+b_{-1}^2)(c_1^2+c_{-1}^2)(b_{-1}(-c_1+c_{-1})+b_1(c_1+c_{-1}))\,(b_1(c_1-c_{-1})$$
$$+b_{-1}(c_1+c_{-1}))\,g_2^2 g_3^2 + (c_1^2+c_{-1}^2)^4 g_3^4 + 8a_1^3 a_{-1} g_1^2 (b_1 b_{-1}(b_1^2+b_{-1}^2)g_2^2 + c_1 c_{-1}(c_1^2+c_{-1}^2)g_3^2)$$
$$+8a_1 a_{-1}^3 g_1^2 (b_1 b_{-1}(b_1^2+b_{-1}^2)g_2^2 + c_1 c_{-1}(c_1^2+c_{-1}^2)g_3^2) + 2a_1^4 g_1^2\,(3a_{-1}^4 g_1^2$$
$$+(b_1^4-b_{-1}^4)g_2^2 + (c_1^4-c_{-1}^4)g_3^2) + 2a_{-1}^4 g_1^2((-b_1^4+b_{-1}^4)g_2^2 + (-c_1^4+c_{-1}^4)g_3^2))^{1/2}\Big)\,.$$

Appendix C. Order parameters, bosonic representation, scaling analysis

In our analysis, the fermionic bilinears for the order parameters are expressed in terms of Gell–Mann matrices, which are a set of eight linearly independent 3×3 traceless Hermitian matrices, given by-

$$\lambda^1 = \begin{pmatrix} 0 & 1 & 0 \\ 1 & 0 & 0 \\ 0 & 0 & 0 \end{pmatrix}, \qquad \lambda^2 = \begin{pmatrix} 0 & -\mathrm{i} & 0 \\ \mathrm{i} & 0 & 0 \\ 0 & 0 & 0 \end{pmatrix}$$

$$\lambda^3 = \begin{pmatrix} 1 & 0 & 0 \\ 0 & -1 & 0 \\ 0 & 0 & 0 \end{pmatrix}, \qquad \lambda^4 = \begin{pmatrix} 0 & 0 & 1 \\ 0 & 0 & 0 \\ 1 & 0 & 0 \end{pmatrix}$$

$$\lambda^5 = \begin{pmatrix} 0 & 0 & -\mathrm{i} \\ 0 & 0 & 0 \\ \mathrm{i} & 0 & 0 \end{pmatrix}, \qquad \lambda^6 = \begin{pmatrix} 0 & 0 & 0 \\ 0 & 0 & 1 \\ 0 & 1 & 0 \end{pmatrix}$$

$$\lambda^7 = \begin{pmatrix} 0 & 0 & 0 \\ 0 & 0 & -\mathrm{i} \\ 0 & \mathrm{i} & 0 \end{pmatrix}, \qquad \lambda^8 = \frac{1}{\sqrt{3}}\begin{pmatrix} 1 & 0 & 0 \\ 0 & 1 & 0 \\ 0 & 0 & -2 \end{pmatrix}.$$

Below, we list the expressions for the eighteen order parameters in terms of the bosonic fields:

$$\mathrm{Re}[O_{\mathrm{ph}}^{00}] \propto \left(2\ \cos[\sqrt{2}\sqrt{\pi}\widetilde{\phi}_1]\sin\left[\frac{2\sqrt{\pi}\widetilde{\phi}_{-1}}{\sqrt{6}} + \frac{2\sqrt{\pi}\widetilde{\phi}_0}{\sqrt{3}} - 2k_{\mathrm{F}}x\right] + \sin\left[-\frac{4}{\sqrt{6}}\sqrt{\pi}\widetilde{\phi}_{-1} + \frac{2\sqrt{\pi}\widetilde{\phi}_0}{\sqrt{3}} - 2k_{\mathrm{F}}x\right]\right)$$

$$\mathrm{Re}[O_{\mathrm{ph}}^{10}] \propto \sin[\sqrt{2}\sqrt{\pi}\widetilde{\theta}_1]\cos\left[\frac{2\sqrt{\pi}\widetilde{\phi}_{-1}}{\sqrt{6}} + \frac{2\sqrt{\pi}\widetilde{\phi}_0}{\sqrt{3}} - 2k_{\mathrm{F}}x\right]$$

$$\mathrm{Re}[O_{\mathrm{ph}}^{20}] \propto \cos[\sqrt{2}\sqrt{\pi}\widetilde{\theta}_1]\cos\left[\frac{2\sqrt{\pi}\widetilde{\phi}_{-1}}{\sqrt{6}} + \frac{2\sqrt{\pi}\widetilde{\phi}_0}{\sqrt{3}} - 2k_{\mathrm{F}}x\right]$$

$$\mathrm{Re}[O_{\mathrm{ph}}^{30}] \propto \sin[\sqrt{2}\sqrt{\pi}\widetilde{\phi}_1]\cos\left[\frac{2\sqrt{\pi}\widetilde{\phi}_{-1}}{\sqrt{6}} + \frac{2\sqrt{\pi}\widetilde{\phi}_0}{\sqrt{3}} - 2k_{\mathrm{F}}x\right]$$

$$\mathrm{Re}[O_{\mathrm{ph}}^{40}] \propto \sin\left[\frac{\sqrt{\pi}\widetilde{\theta}_1}{\sqrt{2}} + \frac{3\sqrt{\pi}\widetilde{\theta}_{-1}}{\sqrt{6}}\right]\cos\left[\frac{\sqrt{\pi}\widetilde{\phi}_1}{\sqrt{2}} - \frac{\sqrt{\pi}\widetilde{\phi}_{-1}}{\sqrt{6}} + \frac{2\sqrt{\pi}\widetilde{\phi}_0}{\sqrt{3}} - 2k_{\mathrm{F}}x\right]$$

$$\mathrm{Re}[O_{\mathrm{ph}}^{50}] \propto \cos\left[\frac{\sqrt{\pi}\widetilde{\theta}_1}{\sqrt{2}} + \frac{3\sqrt{\pi}\widetilde{\theta}_{-1}}{\sqrt{6}}\right]\cos\left[\frac{\sqrt{\pi}\widetilde{\phi}_1}{\sqrt{2}} - \frac{\sqrt{\pi}\widetilde{\phi}_{-1}}{\sqrt{6}} + \frac{2\sqrt{\pi}\widetilde{\phi}_0}{\sqrt{3}} - 2k_{\mathrm{F}}x\right]$$

$$\mathrm{Re}[O_{\mathrm{ph}}^{60}] \propto \sin\left[\frac{\sqrt{\pi}\widetilde{\theta}_1}{\sqrt{2}} - \frac{3\sqrt{\pi}\widetilde{\theta}_{-1}}{\sqrt{6}}\right]\cos\left[\frac{\sqrt{\pi}\widetilde{\phi}_1}{\sqrt{2}} + \frac{\sqrt{\pi}\widetilde{\phi}_{-1}}{\sqrt{6}} - \frac{2\sqrt{\pi}\widetilde{\phi}_0}{\sqrt{3}} + 2k_{\mathrm{F}}x\right]$$

$$\mathrm{Re}[O^{70}_{\mathrm{ph}}] \propto \cos\left[\frac{\sqrt{\pi}\widetilde{\theta}_1}{\sqrt{2}} - \frac{3\sqrt{\pi}\widetilde{\theta}_{-1}}{\sqrt{6}}\right]\cos\left[\frac{\sqrt{\pi}\widetilde{\phi}_1}{\sqrt{2}} + \frac{\sqrt{\pi}\widetilde{\phi}_{-1}}{\sqrt{6}} - \frac{2\sqrt{\pi}\widetilde{\phi}_0}{\sqrt{3}} + 2k_{\mathrm{F}}x\right]$$

$$\mathrm{Re}[O^{80}_{\mathrm{ph}}] \propto \left(\cos[\sqrt{2}\sqrt{\pi}\widetilde{\phi}_1]\sin\left[\frac{2\sqrt{\pi}\widetilde{\phi}_{-1}}{\sqrt{6}} + \frac{2\sqrt{\pi}\widetilde{\phi}_0}{\sqrt{3}} - 2k_{\mathrm{F}}x\right] - \sin\left[-\frac{4}{\sqrt{6}}\sqrt{\pi}\widetilde{\phi}_{-1} + \frac{2\sqrt{\pi}\widetilde{\phi}_0}{\sqrt{3}} - 2k_{\mathrm{F}}x\right]\right)$$

$$\mathrm{Re}[O^{00}_{\mathrm{pp}}] \propto \left(2\ \cos[\sqrt{2}\sqrt{\pi}\widetilde{\theta}_1]\sin\left[\frac{2\sqrt{\pi}\widetilde{\theta}_{-1}}{\sqrt{6}} + \frac{2\sqrt{\pi}\widetilde{\theta}_0}{\sqrt{3}}\right] - \sin\left[\frac{4\sqrt{\pi}\widetilde{\theta}_{-1}}{\sqrt{6}} - \frac{2\sqrt{\pi}\widetilde{\theta}_0}{\sqrt{3}}\right]\right)$$

$$\mathrm{Re}[O^{10}_{\mathrm{pp}}] \propto \sin[\sqrt{2}\sqrt{\pi}\widetilde{\phi}_1]\cos\left[\frac{2\sqrt{\pi}\widetilde{\theta}_{-1}}{\sqrt{6}} + \frac{2\sqrt{\pi}\widetilde{\theta}_0}{\sqrt{3}}\right]$$

$$\mathrm{Re}[O^{20}_{\mathrm{pp}}] \propto \cos[\sqrt{2}\sqrt{\pi}\widetilde{\phi}_1]\cos\left[\frac{2\sqrt{\pi}\widetilde{\theta}_{-1}}{\sqrt{6}} + \frac{2\sqrt{\pi}\widetilde{\theta}_0}{\sqrt{3}}\right]$$

$$\mathrm{Re}[O^{30}_{\mathrm{pp}}] \propto \sin[\sqrt{2}\sqrt{\pi}\widetilde{\theta}_1]\cos\left[\frac{2\sqrt{\pi}\widetilde{\theta}_{-1}}{\sqrt{6}} + \frac{2\sqrt{\pi}\widetilde{\theta}_0}{\sqrt{3}}\right]$$

$$\mathrm{Re}[O^{40}_{\mathrm{pp}}] \propto \sin\left[\frac{\sqrt{\pi}\widetilde{\phi}_1}{\sqrt{2}} + \frac{3\sqrt{\pi}\widetilde{\phi}_{-1}}{\sqrt{6}}\right]\cos\left[\frac{\sqrt{\pi}\widetilde{\theta}_1}{\sqrt{2}} - \frac{\sqrt{\pi}\widetilde{\theta}_{-1}}{\sqrt{6}} + \frac{2\sqrt{\pi}\widetilde{\theta}_0}{\sqrt{3}}\right]$$

$$\mathrm{Re}[O^{50}_{\mathrm{pp}}] \propto \cos\left[\frac{\sqrt{\pi}\widetilde{\phi}_1}{\sqrt{2}} + \frac{3\sqrt{\pi}\widetilde{\phi}_{-1}}{\sqrt{6}}\right]\cos\left[\frac{\sqrt{\pi}\widetilde{\theta}_1}{\sqrt{2}} - \frac{\sqrt{\pi}\widetilde{\theta}_{-1}}{\sqrt{6}} + \frac{2\sqrt{\pi}\widetilde{\theta}_0}{\sqrt{3}}\right]$$

$$\mathrm{Re}[O^{60}_{\mathrm{pp}}] \propto \sin\left[\frac{\sqrt{\pi}\widetilde{\phi}_1}{\sqrt{2}} - \frac{3\sqrt{\pi}\widetilde{\phi}_{-1}}{\sqrt{6}}\right]\cos\left[\frac{\sqrt{\pi}\widetilde{\theta}_1}{\sqrt{2}} + \frac{\sqrt{\pi}\widetilde{\theta}_{-1}}{\sqrt{6}} - \frac{2\sqrt{\pi}\widetilde{\theta}_0}{\sqrt{3}}\right]$$

$$\mathrm{Re}[O^{70}_{\mathrm{pp}}] \propto \cos\left[\frac{\sqrt{\pi}\widetilde{\phi}_1}{\sqrt{2}} - \frac{3\sqrt{\pi}\widetilde{\phi}_{-1}}{\sqrt{6}}\right]\cos\left[\frac{\sqrt{\pi}\widetilde{\theta}_1}{\sqrt{2}} + \frac{\sqrt{\pi}\widetilde{\theta}_{-1}}{\sqrt{6}} - \frac{2\sqrt{\pi}\widetilde{\theta}_0}{\sqrt{3}}\right]$$

$$\mathrm{Re}[O^{80}_{\mathrm{pp}}] \propto \left(\cos[\sqrt{2}\sqrt{\pi}\widetilde{\theta}_1]\sin\left[\frac{2\sqrt{\pi}\widetilde{\theta}_{-1}}{\sqrt{6}} + \frac{2\sqrt{\pi}\widetilde{\theta}_0}{\sqrt{3}}\right] + \sin\left[\frac{4\sqrt{\pi}\widetilde{\theta}_{-1}}{\sqrt{6}} - \frac{2\sqrt{\pi}\widetilde{\theta}_0}{\sqrt{3}}\right]\right). \tag{C1}$$

We further define the order parameters

$$\mathrm{Re}[\Delta^{10}_{\mathrm{ph}}] \propto \sin\left[\sqrt{2}\sqrt{\pi}\widetilde{\phi}_1 + \frac{2\sqrt{\pi}\widetilde{\phi}_{-1}}{\sqrt{6}} + \frac{2\sqrt{\pi}\widetilde{\phi}_0}{\sqrt{3}} - 2k_{\mathrm{F}}x\right]$$

$$\mathrm{Re}[\Delta^{20}_{\mathrm{ph}}] \propto \sin\left[\sqrt{2}\sqrt{\pi}\widetilde{\phi}_1 - \frac{2\sqrt{\pi}\widetilde{\phi}_{-1}}{\sqrt{6}} - \frac{2\sqrt{\pi}\widetilde{\phi}_0}{\sqrt{3}} + 2k_{\mathrm{F}}x\right]$$

$$\mathrm{Re}[\Delta^{30}_{\mathrm{ph}}] \propto \sin\left[\frac{4\sqrt{\pi}\widetilde{\phi}_{-1}}{\sqrt{6}} - \frac{2\sqrt{\pi}\widetilde{\phi}_0}{\sqrt{3}} + 2k_{\mathrm{F}}x\right]$$

$$\mathrm{Re}[\Delta^{10}_{\mathrm{pp}}] \propto \sin\left[\sqrt{2}\sqrt{\pi}\widetilde{\theta}_1 + \frac{2\sqrt{\pi}\widetilde{\theta}_{-1}}{\sqrt{6}} + \frac{2\sqrt{\pi}\widetilde{\theta}_0}{\sqrt{3}}\right]$$

$$\mathrm{Re}[\Delta^{20}_{\mathrm{pp}}] \propto \sin\left[\sqrt{2}\sqrt{\pi}\widetilde{\theta}_1 - \frac{2\sqrt{\pi}\widetilde{\theta}_{-1}}{\sqrt{6}} - \frac{2\sqrt{\pi}\widetilde{\theta}_0}{\sqrt{3}}\right]$$

$$\mathrm{Re}[\Delta^{30}_{\mathrm{pp}}] \propto \sin\left[\frac{4\sqrt{\pi}\widetilde{\theta}_{-1}}{\sqrt{6}} - \frac{2\sqrt{\pi}\widetilde{\theta}_0}{\sqrt{3}}\right]. \tag{C2}$$

corresponding to p–p and p–h ordering on each of the three individual Fermi pockets, which we track in our RG analysis. The order parameters, introduced as infinitesimal test vertices, scale upon renormalization

in the following manner:

$$\frac{dO^{10}_{ph}}{dy} = (2 - \frac{1}{16\pi}((A^{(1)}_1)^2 + (A^{(1)}_{-1})^2 + (a^{(4)}_1)^2 + (a^{(4)}_{-1})^2) + \frac{1}{16\pi}G_1((A^{(1)}_1)^2 + (A^{(1)}_{-1})^2)O^{10}_{ph},$$

$$\frac{dO^{20}_{ph}}{dy} = (2 - \frac{1}{16\pi}((A^{(1)}_1)^2 + (A^{(1)}_{-1})^2 + (a^{(4)}_1)^2 + (a^{(4)}_{-1})^2) - \frac{1}{16\pi}G_1((A^{(1)}_1)^2 + (A^{(1)}_{-1})^2))O^{20}_{ph},$$

$$\frac{dO^{40}_{ph}}{dy} = (2 - \frac{1}{16\pi}((a^{(6)}_1)^2 + (a^{(6)}_{-1})^2 + (A^{(2)}_1)^2 + (A^{(2)}_{-1})^2)) + \frac{1}{16\pi}G_2((A^{(2)}_1)^2 + (A^{(2)}_{-1})^2))\, O^{40}_{ph},$$

$$\frac{dO^{50}_{ph}}{dy} = (2 - \frac{1}{16\pi}((a^{(6)}_1)^2 + (a^{(6)}_{-1})^2 + (A^{(2)}_1)^2 + (A^{(2)}_{-1})^2) - \frac{1}{16\pi}G_2((A^{(2)}_1)^2 + (A^{(2)}_{-1})^2))O^{50}_{ph},$$

$$\frac{dO^{60}_{ph}}{dy} = (2 - \frac{1}{16\pi}((a^{(5)}_1)^2 + (a^{(5)}_{-1})^2 + (A^{(3)}_1)^2 + (A^{(3)}_{-1})^2)) + \frac{1}{16\pi}G_3((A^{(3)}_1)^2 + (A^{(3)}_{-1})^2))\, O^{60}_{ph},$$

$$\frac{dO^{70}_{ph}}{dy} = (2 - \frac{1}{16\pi}((a^{(5)}_1)^2 + (a^{(5)}_{-1})^2 + (A^{(3)}_1)^2 + (A^{(3)}_{-1})^2) - \frac{1}{16\pi}G_3((A^{(3)}_1)^2 + (A^{(3)}_{-1})^2))O^{70}_{ph},$$

$$\frac{d\Delta^{10}_{ph}}{dy} = (2 - \frac{1}{4\pi}(a^2_1 + a^2_{-1}))\Delta^{10}_{ph},$$

$$\frac{d\Delta^{20}_{ph}}{dy} = (2 - \frac{1}{4\pi}(b^2_1 + b^2_{-1}))\Delta^{20}_{ph},$$

$$\frac{d\Delta^{30}_{ph}}{dy} = (2 - \frac{1}{4\pi}(c^2_1 + c^2_{-1}))\Delta^{30}_{ph},$$

$$\frac{dO^{10}_{pp}}{dy} = (2 - \frac{1}{16\pi}((a^{(1)}_1)^2 + (a^{(1)}_{-1})^2 + (A^{(4)}_1)^2 + (A^{(4)}_{-1})^2) + \frac{1}{16\pi}g_1((a^{(1)}_1)^2 + (a^{(1)}_{-1})^2))O^{10}_{pp},$$

$$\frac{dO^{20}_{pp}}{dy} = (2 - \frac{1}{16\pi}((a^{(1)}_1)^2 + (a^{(1)}_{-1})^2 + (A^{(4)}_1)^2 + (A^{(4)}_{-1})^2) - \frac{1}{16\pi}g_1((a^{(1)}_1)^2 + (a^{(1)}_{-1})^2))O^{20}_{pp},$$

$$\frac{dO^{40}_{pp}}{dy} = (2 - \frac{1}{16\pi}((a^{(2)}_1)^2 + (a^{(2)}_{-1})^2 + (A^{(6)}_1)^2 + (A^{(6)}_{-1})^2) + \frac{1}{16\pi}g_2((a^{(2)}_1)^2 + (a^{(2)}_{-1})^2))O^{40}_{pp},$$

$$\frac{dO^{50}_{pp}}{dy} = (2 - \frac{1}{16\pi}((a^{(2)}_1)^2 + (a^{(2)}_{-1})^2 + (A^{(6)}_1)^2 + (A^{(6)}_{-1})^2) - \frac{1}{16\pi}g_2((a^{(2)}_1)^2 + (a^{(2)}_{-1})^2))O^{50}_{pp},$$

$$\frac{dO^{60}_{pp}}{dy} = (2 - \frac{1}{16\pi}((a^{(3)}_1)^2 + (a^{(3)}_{-1})^2 + (A^{(5)}_1)^2 + (A^{(5)}_{-1})^2) + \frac{1}{16\pi}g_3((a^{(3)}_1)^2 + (a^{(3)}_{-1})^2))O^{60}_{pp},$$

$$\frac{dO^{70}_{pp}}{dy} = (2 - \frac{1}{16\pi}((a^{(3)}_1)^2 + (a^{(3)}_{-1})^2 + (A^{(5)}_1)^2 + (A^{(5)}_{-1})^2) - \frac{1}{16\pi}g_3((a^{(3)}_1)^2 + (a^{(3)}_{-1})^2))O^{70}_{pp},$$

$$\frac{d\Delta^{10}_{pp}}{dy} = (2 - \frac{1}{4\pi}(A^2_1 + A^2_{-1}))\Delta^{10}_{pp},$$

$$\frac{d\Delta^{20}_{pp}}{dy} = (2 - \frac{1}{4\pi}(B^2_1 + B^2_{-1}))\Delta^{20}_{pp},$$

$$\frac{d\Delta^{30}_{pp}}{dy} = (2 - \frac{1}{4\pi}(C^2_1 + C^2_{-1}))\Delta^{30}_{pp}, \tag{C3}$$

where the coefficients of the fields $\widetilde{\phi}_i$ and $\widetilde{\theta}_i$ in the sine-Gordon terms representing the different order parameters O^{i0}_{ph}, O^{i0}_{pp} are expressed in terms of $a^{(\alpha)}_i, \alpha = 1$–$6$ and $A^{(\alpha)}_i, \alpha = 1$–$3$ respectively. Note that we work in the regimes $K^{\phi}_0 \gg K^{\phi}_{\perp}$ or $K^{\phi}_0 \ll K^{\phi}_{\perp}$, which enables us to drop terms involving K^{ϕ}_0 compared to those involving $K^{\phi}_{\perp}$, in different regimes.

Here $a^{(\alpha)}_i, \alpha = 1$–$6$ and $A^{(\alpha)}_i, \alpha = 1$–$3$ are the usual coefficients of the fields for the interaction couplings g_α as defined in equation (4) of the main text. On the other hand, the coefficients $A^{(\alpha)}_i, \alpha = 4$–$6$ are defined in the same way for the fields $\widetilde{\theta}_i$ as $a^{(\alpha)}_i, \alpha = 4$–$6$ are defined for the fields $\widetilde{\phi}_i$ in equation (4). While the latter coefficients for the fields $\widetilde{\theta}_i$ do not actually appear in the sine-Gordon terms corresponding to any of the interaction couplings considered by us in equation (4), we introduce them here for simplicity, since the

coefficients of the fields in some of the order parameters can be expressed neatly in terms of these quantities.

In addition, the coefficients of the fields for the sine-Gordon terms corresponding to the order parameters $\Delta^{i0}_{\rm pp/ph}(i=1\text{–}3)$ (see equation (C2) above) are defined as a_i, b_i, c_i and A_i, B_i, C_i (where $i=1,-1$), as these cannot be expressed in terms of the coefficients already defined for any of the interaction couplings g_α in equation (4). Note that the scaling dimensions for these order parameters do not have any $O(g)$ corrections from any of the nine couplings $g_i, i=1\text{–}6$, $G_i, i=1\text{–}3$ considered by us. However there are $O(g)$ corrections to their scaling dimensions from other interaction terms with higher scaling dimensions that have been neglected in this analysis. The order parameters $\Delta^{i0}_{\rm pp/ph}(i=1\text{–}3)$ simultaneously diverge in certain parameter regimes where $K^\phi_\perp$ takes extremely large or small values (depending on the type of order being considered). The specific nature of order in these phases requires consideration of higher order processes that couple the degenerate order parameters, and may have s-wave, d-wave or chiral d-wave symmetry (see main text for discussion).

Appendix D. Estimation of coupling constants for semimetals at high magnetic fields

Below, we attempt to obtain an estimate for the factors that may determine the strength of the couplings and Luttinger parameters in a semimetal with three small Fermi pockets at high magnetic fields. The fermionic couplings are essentially derived from the screened Coulomb interactions within each Fermi pocket, as well as those between different pockets. The screened Coulomb interaction within the three electron pockets is given by $U^e_0(r)=\frac{e^2}{4\pi\epsilon\epsilon_0 r}\exp(-r/\lambda_{\rm TF})$, where ϵ is the dielectric constant in the absence of conduction charges and $\lambda_{\rm TF}$ is the Thomas–Fermi screening length. In momentum space, we have the corresponding expression $V^e_0(\mathbf{q})=\frac{e^2}{\epsilon\epsilon_0(q^2+\lambda_{\rm TF}^{-2})}$, which is the Fourier transform of $U^e_0(r)$. Now, the Luttinger parameter $K^\phi_\perp$ for a given Luttinger liquid system is governed by the various intraband scattering processes. The forward-scattering processes within a given band, corresponding to a momentum transfer $q\sim 0$, are determined by $V^e_0(0,0,0)=\frac{e^2\lambda^2_{\rm TF}}{\epsilon\epsilon_0}$. The backscattering processes between different Fermi points $\pm k_{\rm F}$ within a given band, are determined by $V^e_0(0,0,2k_{\rm F})=\frac{e^2}{\epsilon\epsilon_0((2k_{\rm F})^2+\lambda_{\rm TF}^{-2})}$. On the other hand, the sine-Gordon couplings, which we assume to be perturbatively small, are derived from weaker scattering processes between different bands. The backscattering and Umklapp processes between different bands are given by a momentum transfer $Q\gg k_{\rm F}$ (see figure 2 of the paper for a pictorial depiction of the separation of the Luttinger liquid systems in momentum space), i.e. $V^e_0(Q)=\frac{e^2}{\epsilon\epsilon_0(Q^2+\lambda_{\rm TF}^{-2})}$.

For determining if these couplings correspond to the strong or weak correlation regime, we must compare them with corresponding kinetic energy scales, and the dimensionless interaction couplings are given by the product of $V^e_0(\mathbf{q})$ and the density of states at the Fermi level. In the quantum limit, the kinetic energy is completely quenched in the plane perpendicular to the magnetic field, since the particles execute bound motion with localization length $l_{\rm B}=\sqrt{\frac{\hbar}{eB}}$. This leads to an increase in the dimensionless interaction strength due to the resultant increase in the density of states. Then the dimensionless coupling constant corresponding to forward-scattering processes within a band, denoted by g, is defined as the product of the Coulomb interaction and the density of states, i.e.

$$g=V^e_0(0,0,0)\times(1/(l_{\rm B}^2))\times(1/(2\pi\hbar v_{\rm F}))=(4\pi e^2/4\pi\epsilon\epsilon_0\hbar c)\times(\lambda^2_{\rm TF}/(l_{\rm B}^2))\times(c/(2\pi v_{\rm F}))$$
$$=(2/(137\epsilon))\times(\lambda^2_{\rm TF}/l_{\rm B}^2)\times(c/v_{\rm F})=(2/(137\epsilon))\times(\lambda^2_{\rm TF}eB/h)\times(c/v_{\rm F}).$$

Thus, the dimensionless interaction strength increases with increasing field B, and it becomes strong once the magnetic length $l_{\rm B}$ falls below the Thomas–Fermi screening length $\lambda_{\rm TF}$, and when the Fermi velocity of the 1D fermions is small, i.e. $v_{\rm F}/c\ll 1$.

In the specific case of bismuth, the quantum limit is reached for fields around 9 T, given a carrier density of 3×10^{17} cm^{-3}, average electron velocity $v_{\rm F}=3.5\times10^5$ m s^{-1} and dielectric constant $\epsilon=30$ [63]. This gives $g\approx 0.4\times(\lambda_{\rm TF}/l_{\rm B})^2$. The Thomas–Fermi screening length is of the order of r_0, the inter-electron distance. These interaction couplings enter into the Luttinger parameter $K^{\theta,\phi}$ discussed in the paper, since they correspond to $q=(0,0,0)$. For $k_{\rm F}\approx\lambda^{-1}_{\rm TF}$, the corresponding process involving a momentum transfer of $2k_{\rm F}$ is at least five times weaker. On the other hand, a smaller value of the coupling $V^e_0(Q)$ from interband scattering processes enters the sine-Gordon terms. As described in the main text, we generally consider weak repulsive sine-Gordon interactions in our approach, since these are derived from the Coulomb interaction at large momenta.

ORCID iDs

S Kundu https://orcid.org/0000-0003-0113-6236
V Tripathi https://orcid.org/0000-0002-7771-8550

References

[1] Nishimoto S, Jeckelmann E and Scalapino D J 2009 *Phys. Rev.* B **79** 205115
[2] Fjærestad J O and Marston J B 2002 *Phys. Rev.* B **65** 125106
[3] Nishimoto S, Jeckelmann E and Scalapino D J 2002 *Phys. Rev.* B **66** 245109
[4] Lee S, Marston J B and Fjærestad J O 2005 *Phys. Rev.* B **72** 075126
[5] Chudzinski P, Gabay M and Giamarchi T 2007 *Phys. Rev.* B **76** 161101
[6] Chudzinski P, Gabay M and Giamarchi T 2008 *Phys. Rev.* B **78** 075124
[7] Tsuchiizu M and Furusaki A 2002 *Phys. Rev.* B **66** 245106
[8] Wessel S, Indergand M, Läuchli A, Ledermann U and Sigrist M 2003 *Phys. Rev.* B **67** 184517
[9] Wu C, Vincent Liu W and Fradkin E 2003 *Phys. Rev.* B **68** 115104
[10] O'Hern C S, Lubensky T C and Toner J 1999 *Phys. Rev. Lett.* **83** 2745
[11] Suzumura Y and Tsuchiizu M 2001 *J. Phys. Chem. Solids* **62** 93
[12] Chen S, Buttner H and Voit J 2001 *Phys. Rev. Lett.* **87** 087205
[13] Vincent Liu W and Fradkin E 2001 *Phys. Rev. Lett.* **86** 1865
[14] Sheng D N, Motrunich O I and Fisher M P A 2009 *Phys. Rev.* B **79** 205112
[15] Sato M 2007 *Phys. Rev.* B **76** 054427
[16] Shelton D G, Nersesyan A A and Tsvelik A M 1996 *Phys. Rev.* B **53** 8521
[17] Khveshchenko D V and Rice T M 1994 *Phys. Rev.* B **50** 252
[18] Cabra D C, Honecker A and Pujol P 2000 *Eur. Phys. J.* B **13** 55
[19] Allen D, Azaria P and Lecheminant P 2001 *J. Phys. A: Math. Gen.* **34** L305
[20] Le Hur K, Soret A and Yang F 2017 *Phys. Rev.* B **96** 205109
[21] Okamoto J-i and Millis A J 2012 *Phys. Rev.* B **85** 115406
[22] Carpentier D and Orignac E 2006 *Phys. Rev.* B **74** 085409
[23] DeGottardi W, Wei T-C, Fernández V and Vishveshwara S 2010 *Phys. Rev.* B **82** 155411
[24] Orignac E, Citro R and Andrei N 2000 *Phys. Rev.* B **61** 11533
[25] Sato M 2007 *Phys. Rev.* B **75** 174407
[26] Charrier D, Capponi S, Oshikawa M and Pujol P 2010 *Phys. Rev.* B **82** 075108
[27] Zhao Y, Gong S-S, Wang Y-J and Su G 2012 *Phys. Rev.* B **86** 224406
[28] Fuji Y, Nishimoto S, Nakada H and Oshikawa M 2014 *Phys. Rev.* B **89** 054425
[29] Plat X, Fuji Y, Capponi S and Pujol P 2015 *Phys. Rev.* B **91** 064411
[30] Arrigoni E 1996 *Phys. Status Solidi b* **195** 425
[31] Arrigoni E 1996 *Phys. Lett.* A **215** 91
[32] Kimura T, Kuroki K and Aoki H 1996 *Phys. Rev.* B **54** R9608
[33] Kimura T, Kuroki K and Aoki H 1998 *J. Phys. Soc. Japan* **67** 1377
[34] Miao J-J, Zhang F-C and Zhou Y 2016 *Phys. Rev.* B **94** 205129
[35] Kallin C and Berlinsky J 2016 *Rep. Prog. Phys.* **79** 054502
[36] Behnia K, Balicas L and Kopelevich Y 2007 *Science* **317** 1729
[37] Fauqué B, Vignolle B, Proust C, Issi J-P and Behnia K 2009 *New J. Phys.* **11** 113012
[38] Küchler R, Steinke L, Daou R, Brando M, Behnia K and Steglich F 2014 *Nat. Mater.* **13** 461
[39] Li L, Checkelsky J G, Hor Y S, Uher C, Hebard A F, Cava R J and Ong N P 2008 *Science* **321** 547
[40] Sharlai Y V and Mikitik G P 2009 *Phys. Rev.* B **79** 081102
[41] Alicea J and Balents L 2009 *Phys. Rev.* B **79** 241101
[42] Fauqué B, Yang H, Sheikin I, Balicas L, Issi J-P and Behnia K 2009 *Phys. Rev.* B **79** 245124
[43] Matsuo M, Endo A, Hatano N, Nakamura H, Shirasaki R and Sugihara K 2009 *Phys. Rev.* B **80** 075313
[44] Zhu Z, Fauqué B, Fuseya Y and Behnia K 2011 *Phys. Rev.* B **84** 115137
[45] Seradjeh B, Wu J and Phillips P 2009 *Phys. Rev. Lett.* **103** 136803
[46] Yang H, Fauqué B, Malone L, Antunes A B, Zhu Z, Uher C and Behnia K 2010 *Nat. Commun.* **1** 47
[47] Zhu Z, Fauqué B, Malone L, Antunes A B, Fuseya Y and Behnia K 2012 *Proc. Natl Acad. Sci. USA* **109** 14813
[48] Dresselhaus M S and Dresselhaus G 1981 *Adv. Phys.* **30** 139
[49] Vogel F L 1979 Intercalation compounds of graphite *Molecular Metals* ed W E Hatfield (Berlin: Springer) pp 261–79
[50] Rao S and Sen D 2001 arXiv:cond-mat/0005492
[51] von Delft J and Schoeller H 1998 *Ann. Phys., Lpz.* **7** 225
[52] Assaraf R, Azaria P, Caffarel M and Lecheminant P 1999 *Phys. Rev.* B **60** 2299
[53] Tsukamoto Y, Kawakami N, Yamashita Y and Ueda K 2000 *Physica* B **281–282** 540
[54] Itoi C, Qin S and Affleck I 2000 *Phys. Rev.* B **61** 6747
[55] Azaria P, Boulat E and Lecheminant P 2000 *Phys. Rev.* B **61** 12112
[56] Lee H C, Azaria P and Boulat E 2004 *Phys. Rev.* B **69** 155109
[57] Azaria P, Gogolin A O, Lecheminant P and Nersesyan A A 1999 *Phys. Rev. Lett.* **83** 624
[58] Schulz H J 1991 *Int. J. Mod. Phys.* B **05** 57
[59] Ejima S, Gebhard F and Nishimoto S 2005 *Europhys. Lett.* **70** 492
[60] Mila F and Zotos X 1993 *Europhys. Lett.* **24** 133
[61] Shirakawa T and Jeckelmann E 2009 *Phys. Rev.* B **79** 195121
[62] Sano K and Ōno Y 2007 *Phys. Rev.* B **75** 113103
[63] Ruhman J and Lee P A 2017 *Phys. Rev.* B **96** 235107